STUDY OF ARROW WAVEGUIDE FABRICATION PROCESS FOR IMPROVING SCATTERING LOSSES

D. O. Carvalho, S. L. Aristizábal, K. F. Albertin, H. Baez and M. I. Alayo
PSI, University of São Paulo
CP 61548, CEP 05424-970, São Paulo, SP, Brazil
dorquiza@lme.usp.br, slopera@lsi.usp.br, franklin@lme.usp.br, hebame@lme.usp.br, malayo@lme.usp.br

Abstract

A study of scattering losses on the side-walls of Anti-Resonant Reflecting Optical Waveguides (ARROW) is presented in this work. The waveguides were fabricated using SiO_xN_y films deposited by Plasma Enhanced Chemical Vapor Deposition (PECVD) at low temperatures (~300°C). Two different materials were used for the fabrication of the first anti-resonant layer: a-SiC:H films deposited by PECVD and TiO_x films deposited by sputtering technique. To design the ARROW structures, homemade routines based in two computational methods were developed: the Transfer Matrix Method (TMM) for the determination of the optimum thickness values of the Fabry-Perot layers, and the Non-Uniform Finite Difference Method (NU-FDM) for 2D design and determination of the maximum width that allows single-mode operation. In contrast to usual FDM, in NU-FDM the size of the grid cells may vary, which makes it more suited for ARROW waveguides. For the optical characterization the top view technique was used to measure the propagation losses for working wavelength of 633 nm. Also, results of the modal analysis for the determination the maximum rib width that allows the cutoff of the superior modes are presented. Finally, preliminary results of fabrication process modifications for improving the scattering losses are presented.

Keywords: ARROW waveguides, scattering losses, integrated optics, optical devices, PECVD

Introduction

Over the past years, Anti-Resonant Reflecting Optical Waveguides (ARROW) have been used in different Integrated Optics applications [1, 2, 3]. In this kind of structure, light guiding is partially achieved through anti-resonant reflections in properly designed cladding layers which must satisfy the anti-resonant condition for the wavelength of the propagating light [4]. Due to this, ARROW waveguides present some unique characteristics, such as virtual single-mode operation, polarization sensitivity and relaxed fabrication tolerances, which make them more attractive than conventional waveguides for the fabrication of interferometric, absorbance, refratometric, accelerometric and biological sensors [1, 2, 3]. Also, these characteristics make ARROW waveguides an interesting choice for other kinds of devices such as optical polarizers and lasers [5,6].

One of the great advantages of this type of device, over conventional waveguides, is the possibility of single-mode operation with relatively large core thicknesses, compatible with optical fiber diameter, and, at the same time, a much smaller cladding thickness. The fabrication tolerance, related to thickness and refractive index values of the layers, is very large, in contrast to conventional waveguides, where either very small core thickness or small refractive index difference is required in order to obtain single-mode operation. Furthermore, the refractive index of the core layer can be lower than the cladding layers, making the development of hollow core and liquid core waveguides possible [7].

In previous works we reported on the fabrication process of ARROW waveguides, using PECVD silicon oxynitride (SiO_xN_y) films in the fabrication of the core and second ARROW layer [8, 9]. In these works, two different films were used for the fabrication of the first ARROW layer: PECVD amorphous hydrogenated silicon carbide (a-SiC:H) and sputtered titanium oxide (TiO_x) films. The waveguides were fabricated in rib configuration, geometrically defined by reactive ion etching (RIE) technique, using chromium film as masking layer. In these

waveguides it was observed that the wet etching of the chromium film, used as mask, resulted in irregular boundaries.

A comparison of the total losses measured for the waveguides and the scattering loss values calculated by a simple model presented in [10] indicate that the propagation losses due to scattering in the sidewalls of these waveguides have a great contribution in the total losses, as will be shown over the next sessions. For this reason, methods for improving sidewall roughness are proposed and the preliminary results of these methods are presented in this work.

Numerical Simulations

The transfer matrix method (TMM) [11] is an array based calculation method for determining the number of guided and leaky modes, the effective index and the loss for each mode for a given SLAB step index optical waveguide. The loss of each leaky mode can be calculated through the imaginary part of the effective index. In this work, a TMM was implemented and used for the determination of the appropriate thickness of the first anti-resonant layers, which is a very thin layer that works as a Fabry-Perot resonator in anti-resonance and is located just below the core.

Two different kinds of waveguides were simulated and fabricated: waveguides with first ARROW layer composed of sputtered TiO_x (n=2.42) and PECVD a-SiC:H (n=2.10). The other layers in the TMM simulations were: a 2 μm-thick PECVD-SiO_xN_y upper cladding layer (n=1.525); a 4 μm-thick PECVD-SiO_xN_y core (n_c=1.549); a 2 μm-thick PECVD-SiO_xN_y second ARROW layer (n=1.549). The two outer media were air (n=1.00) and silicon substrate (n_{Si}=3.88+0.02i). The thickness of the first ARROW layer in the TMM simulations was varied in order to obtain the minimum loss in these structures. The refractive indexes of the films used in the simulation were experimentally determined by ellipsometry technique.

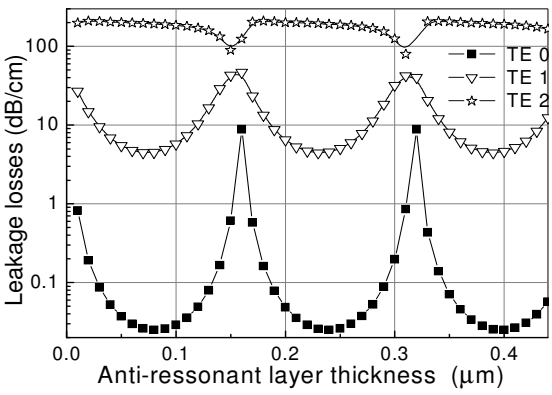

(a)

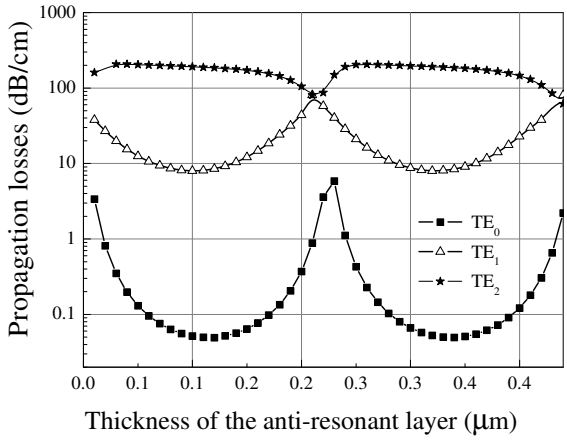

(b)

Figure 1 - TMM results for the optical losses as a function of the anti-resonant-layer thickness for the TiO_x (a) and a-SiC:H (b)waveguides.

The optical losses of the three lowest order TE modes were plotted in Fig. 1a, as a function of the thickness of the TiO_2-first cladding layer. As it can be seen in the figure, thickness values of 90 nm and 240 nm, which correspond to the anti-resonance thicknesses, produce the lowest losses of the zero order TE mode, while the attenuation of the higher order modes is almost 100 times higher than the zero order mode. In the figure, it can also be seen that the leakage loss values of the fundamental mode, for anti-resonance thicknesses, are around 0.025 dB/cm. For the a-SiC:H waveguides the corresponding loss value was somewhat greater (0.049 dB/cm) for thickness values of 0.12 and 0.34 μm (Fig. 1b).

The non-uniform finite difference (NU-FDM) method [12] was implemented and used to design the parameters of the cross section of the rib waveguides, namely the rib height and width. In contrast to usual FDM, in NU-FDM the size of the grid cells may vary.

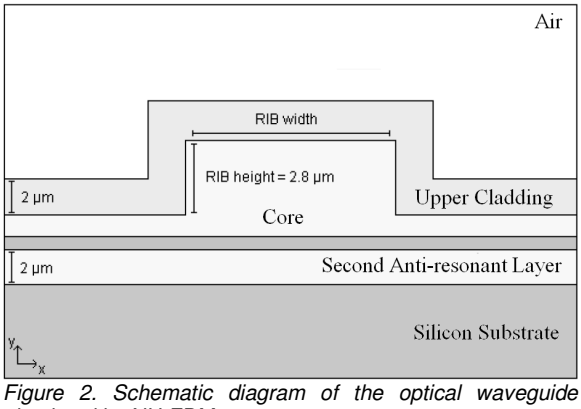

Figure 2. Schematic diagram of the optical waveguide simulated by NU-FDM.

Since the modes propagating in the ARROW structures are modeled through leaky modes, some kind of absorbing or transparent boundary

condition is needed in the bottom of the computational domain. With this purpose we have implemented the perfectly matched layer (PML) based on the complex mapping of space into the complex domain for effectively absorbing the leaky field with negligible reflection [13]. The geometry of the computational domain is shown on Fig. 2a. This domain was divided, in the x direction in 40 points, and in the y direction in 55 points. Also, due to the small thickness of the TiO_2 first ARROW layer, the size of the grid cells was made smaller in order to fit five calculation points in each layer.

ARROW waveguides with different rib height were simulated and the results showed that the deeper the rib height, the lower the leakage loss became. Also, as the rib height decreases, a smaller width is required in order to obtain single-mode operation, as illustrated in Fig. 3, for the TiO_x waveguides, where the leakage losses of the q-TE polarization modes are plotted as a function of the rib width, for rib heights of 0.8 μm (a) and 2.5 μm (b). For this reason, a rib height of 2.8 μm was chosen in order to have single-mode operation with width values that were not too small for our fabrication limits.

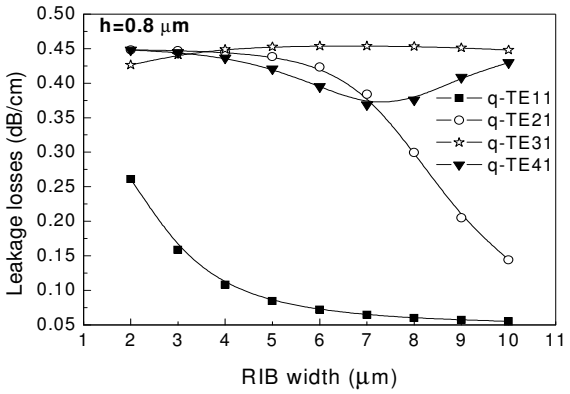

(a)

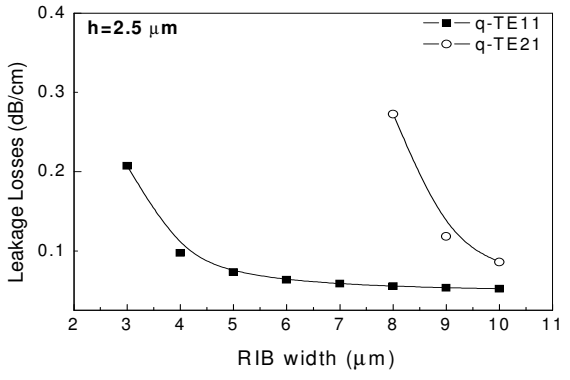

(b)

Figure 3. Leakage losses calculated through NU-FDM, as a function of rib width, for q-TE modes, in TiO_2 waveguides with rib heights of: (a) 0.8 μm and, (b) 2.5 μm.

The results of the FDM simulations were also used to estimate the loss due to scattering on the sidewalls of the waveguides, using the same model as used in [14]. In this model, it is assumed that the scattering losses in rib waveguides are mainly due to sidewall roughness, because the roughness that results from the definition of the sidewalls, in the fabrication processes such as the one used here, is orders of magnitude greater than the surface roughness of the films.

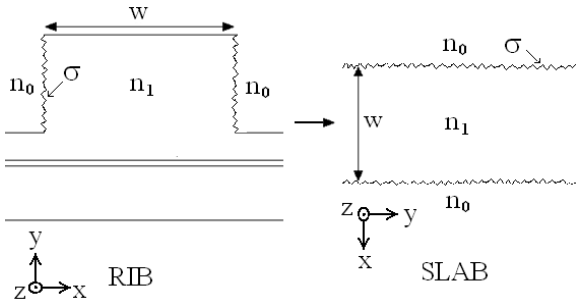

Figure 4. Illustration of the model used in the calculation of the losses due to sidewall scattering.

By modeling the waveguide as a SLAB equivalent, along the lateral direction, with the thickness of the SLAB equal to the width of the actual rib waveguide, as illustrated in Fig. 4, the scattering loss is given by:

$$\alpha_{scattering} = 4.34 \cdot (\beta \cdot \sigma)^2 \frac{\cos^2(\theta)/\mathrm{sen}(\theta)}{w + 2/k_X} \quad (1)$$

In equation 1, β is the propagation constant, $k_x = \sqrt{k^2 - \beta^2}$ is the x component of the wavevector $\vec{k}$, σ is the roughness of the sidewalls, w is the width of the rib waveguide and θ is the angle between the wave vector of the modal solution and the z axis (direction of invariance in the NU-FDM simulation).

Waveguide Fabrication

As shown in previous works by our group, nitrogen and oxygen atomic concentration in PECVD-SiO_xN_y films can be varied continuously by changing the flow ratio of the gases involved in the deposition process [15,16]. Since the refractive index of the SiO_xN_y films is strongly dependent on atomic composition [17,18], there is the possibility of controlling the refractive index of these materials. Silicon oxynitride films with different compositions for the core (n=1.549) and the upper cladding layer (n=1.525) were deposited in a standard 13.56 MHz RF PECVD capacitively coupled system [19].

The gases used in the deposition of these films were silane (SiH_4), nitrous oxide (N_2O) and nitrogen (N_2), and the temperature and the RF power density were maintained constant at

320°C and 500 mW.cm^{-1}, respectively. The substrate was a single crystal silicon, p-type, (100) crystallographic orientation, and resistivity around 1-10 ohm-cm [20].

The first step in the fabrication process was the deposition, on silicon substrate, of a 2 µm-thick silicon oxynitride film with n=1.549. Then, the first ARROW layer was deposited. This layer was an 86 nm-thick TiO_x film, with a similar thickness as the one obtained by the simulations, deposited by Sputtering technique as presented and explained in previous works [11]. The third step was the deposition of the 4 µm-thick core layer, using a silicon oxynitride film with the same composition of the second cladding layer.

The lateral dimensions of the waveguides were defined by optical contact lithography and transferred to the core layer by Reactive Ion Etching (RIE) technique using CHF_3 and O_2. The etching process was done with 200 W of RF power, CHF_3 flow of 40 sccm, O_2 flow of 40 sccm and pressure of 150 mTorr. Sputtered chromium was used as masking layer due to its resistance to CHF_3 and O_2 plasma (20). After a photolithographic process, the chromium mask was defined by wet etching of the chromium layer. The next step was the RIE-etching of the rib, which was followed by the removal of the chromium mask. As mentioned in the previous section, the optical waveguides were fabricated with rib height of 2.8 µm. Finally a PECVD-SiO_xN_y film was deposited as the upper cladding layer. The mask utilized for the definition of the lateral geometry allowed the fabrication of ARROW waveguides with widths from 2 up to 10 µm.

A rough-hewing process followed by polishing of the two lateral faces, where light is coupled into the waveguide (face indicated by the arrow in Fig. 5) and out of the waveguides (opposite side), was performed in order to minimize the optical losses due to the insertion of the light into the waveguides [21].

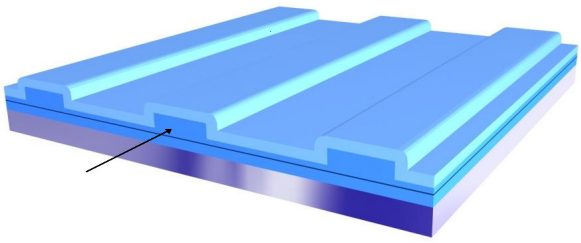

Figure 5. Illustration of the waveguides fabricated with the described process.

Results

The core of the waveguides obtained with the described deposition process before the deposition of the upper cladding are shown in Fig. 6a for waveguides with widths from 7 to 10 µm, and Fig. 6b for a waveguide with a core width of 8 µm, where the roughness on the sidewall of the waveguides can be observed in more detail. Based in this figure, the roughness is estimated to be around values between 50 nm and 80 nm. These values will be used in the scattering losses calculation in the next session.

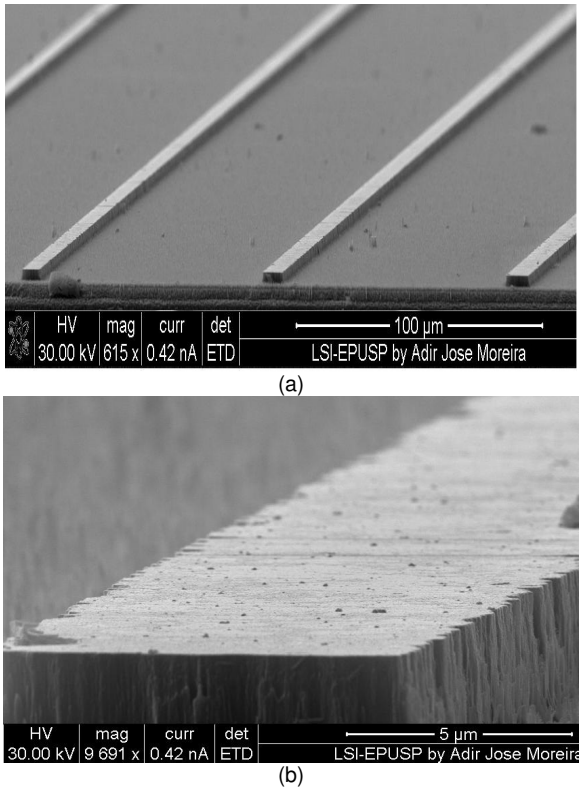

Figure 6. (a) SEM micrographs of waveguides with widths from 7 to 10 µm, before the deposition of the upper cladding layer and (b) the core's surface of an 8 µm-wide waveguide.

Modal distribution measurements for the ARROW waveguides with widths from 3 to 10 µm were achieved using a microscope objective and a charge-coupled device (CCD) camera, as illustrated in Fig. 7. For this, light from a He–Ne laser (632.8 nm) was coupled into a single mode optical fiber (4 µm core diameter) using a microscope objective (20x). Then, the tapered-end of this optical fiber was aligned to one of the polished ends of the optical waveguide (end-fire coupling). The output light of the optical device is shone on a CCD camera (camera number 1, in Fig. 7) using a microscope objective (40x) to capture the intensity profile of the existing modes. Micro-translation stages were used for the accurate alignment of the input fiber, the optical waveguides and the objectives.

The 3-D surface plot of the output light intensity distribution (obtained with the help of an image editing software) for optical waveguides with widths of 8, 9 and 85 µm are shown in Fig. 8a, b and c, respectively. The image captured by the CCD camera is also shown on the left side of each figure.

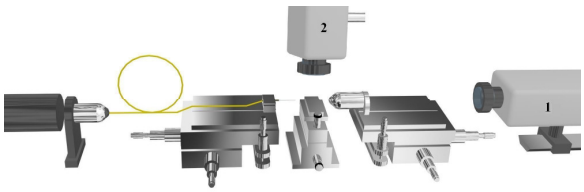

Figure 7 - Experimental setup used for the modal analysis and for the Top View loss measurements (camera 2 above the micro-translation stages).

Waveguides with widths equals or narrower than 8 μm have only the fundamental mode. However, in the optical waveguides with 9 μm in width, it was possible to observe one or two horizontal lobes, depending on the position of the light injecting optical fiber with respect to the input end of the waveguide, which are related to the q-TE_{11} and q-TE_{21} modes [22]. These results are reasonable, when compared with the simulated ones shown in Fig. 3b, where the cutoff of the q-TE_{21} mode happened for waveguides with widths of 7 μm or narrower. This is not contradictory since some over-etching happened in the definition of the chromium mask used in the fabrication of the waveguides, resulting in structures with smaller widths. In the case of the waveguide with rib width of 85 μm (Fig. 8c), the presence of many lateral lobes can be observed.

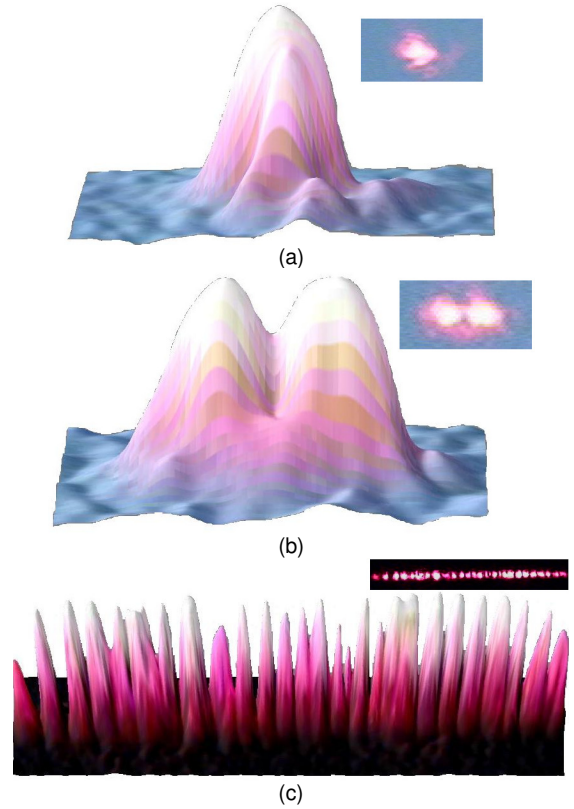

(a)

(b)

(c)

Figure 8. Images captured by CCD camera and 3-D surface plot of the output light intensity for waveguides with widths of: 8 μm (a), 9 μm (b) and 85 μm (c).

In Fig. 8c, it is interesting to observe that even for large widths, the number of lobes is one along the direction transverse to the substrate (y axis in Fig. 2), which means that due to the anti-resonant structure, the higher order modes along this direction, are effectively filtered due to leakage.

For the optical attenuation characterization using the top-view technique [23], a microscope and a CCD camera (camera number 2, in Fig. 6) were positioned above the central micro-translation stage, in order to view the surface of the ARROW structures. Based in the scattered light intensity profile along with the length of the waveguides, obtained from the CCD camera, the optical losses were calculated from the slope of the linear fitting of the resulting curve. This technique is based on the assumption that the scattered light intensity observed from top-view of the waveguide is directly proportional to the propagating light intensity in the waveguide. According to [23] this is a very reasonable assumption if specific irregularities in the waveguide's top surface are not present.

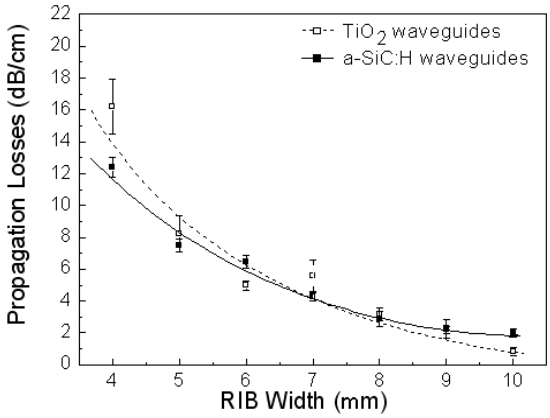

Figure 9. Optical losses (dB/cm) as a function of the waveguide's width (μm) for the TiO_2 and a-SiC:H ARROW structures.

Figure 9 shows the optical losses, measured in dB/cm, as a function of the waveguide width for the TiO_2 and the a-SiC:H ARROW structures. As can be seen, both TiO_2 and a-SiC:H waveguides presented acceptable optical losses for widths larger than 6 μm. In particular, for the widest ARROW structure that allows single-mode operation (widths of about 8 μm), the optical loss was of about 2 dB/cm. The minimum optical loss obtained was of 0.87dB/cm corresponding to a 10-μm TiO_2 ARROW waveguide, which is smaller than the loss for an a-SiC:H waveguide of the same width (1.99 dB/cm). As the rib width increases, the measured propagation losses of the TiO_2 waveguides tend to be greater than the losses of the a-SiC:H waveguides, which is coherent with the TMM simulation results, for SLAB waveguides. The effect of the roughness of the lateral walls seem to increase, with decreasing

rib width, and the fact that the TiO_2 presents a higher reflectance is not as relevant in the total losses, for small widths. Lower optical losses could be attained if a better definition of the vertical walls can be achieved.

The scattering loss curves, calculated through equation 1, for the a-SiC:H waveguides as a function of the rib width can be seen in Fig. 10, along with the measured losses of the a-SiC:H waveguides. The different curves correspond to three different roughnesses: 50, 60 and 70 nm. As mentioned, these values were estimated based on the SEM micrograph shown in Fig. 6b. The values of the measured propagation losses present the same behavior, and have values that are close to the calculated ones, for these values of roughness. These results indicate that the propagation losses, in these waveguides, are mostly due to scattering. Other sources of attenuation, such as leakage and light absorption, have much smaller contribution to the propagation losses. It should be noted, as said before, that as the rib widths decrease, the greater the influence of the loss due to scattering on the sidewalls.

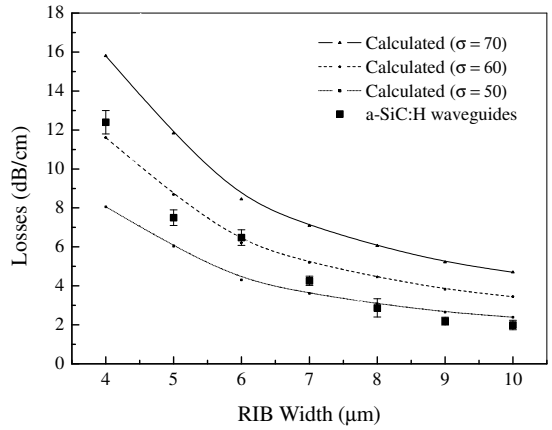

Figure 10.Calculated scattering losses (dB/cm) for three different roughness values (50, 60 and 70 nm), along with the measured values for the a-SiC:H waveguides.

The results presented in Fig. 10 corroborate with the hypothesis that improving the sidewall roughness of the waveguide could further diminish the propagation losses. For this reason, a study of this roughness is being carried out.

Figure 11 shows SEM micrographs of SiO_xN_y films, with the same composition and thickness as the one used for the core of the ARROW waveguides, after reactive ion etching. These films have gone through different chemical treatments, consisting in immersing the etched films in different solutions, namely: trichloroethylene, acetone and isopropyl alcohol (Fig. 11a); standard RCA process (Fig 11b); 30 minutes in a potassium hydroxide solution (KOH) (Fig. 11c); and 10 seconds in a Buffered Oxide Etching (BOE) solution (HF + NH_4F (1:6)) (Fig. 11d).

The first treatment used did not result in any real improvement in the sidewalls of the etched SiO_xN_y or in the etched surface, when compared to films that have not gone through any treatment. In Fig. 11a, grass-like structure is observed in the etched surface, which at first was attributed to polymer formation during the RIE process. Energy dispersive x-ray spectroscopy (EDS) analysis results, however, do not show the presence of carbon in the local composition of this material, indicating that this composition is the same as that of the SiO_xN_y films. According to [24], this grass-like structure results from chromium micro-masking, which takes place in the RIE process due to sputtering of the original chromium mask, and subsequent re-deposition all over the surface of the film.

The RCA cleaning (Fig. 11b) removed part of the grass-like structure, though it did not show any real improvement in the sidewall. Both the KOH solution (Fig. 11c), and the the BOE (Fig. 11d) resulted in partial removal of the grass-like structure, and in some etching of the SiO_xN_y sidewalls, though no significant improvement on the roughness could be observed.

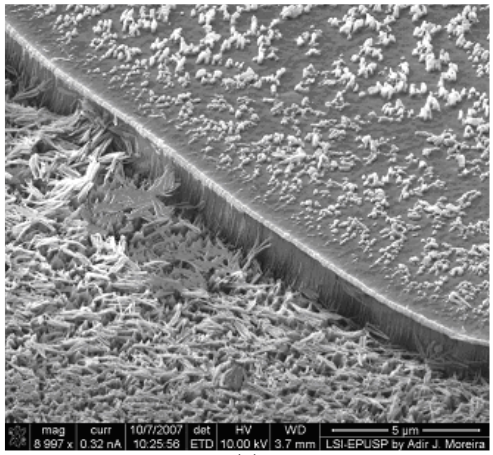

(a)

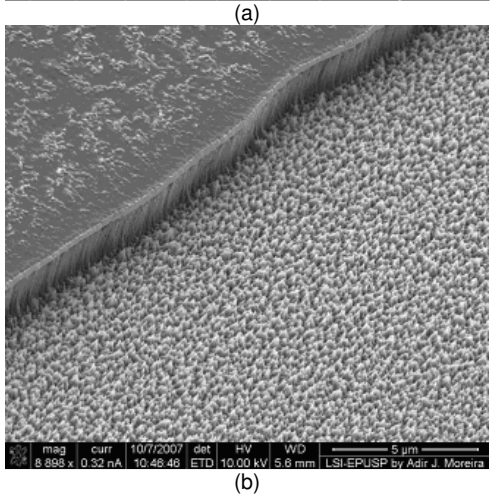

(b)

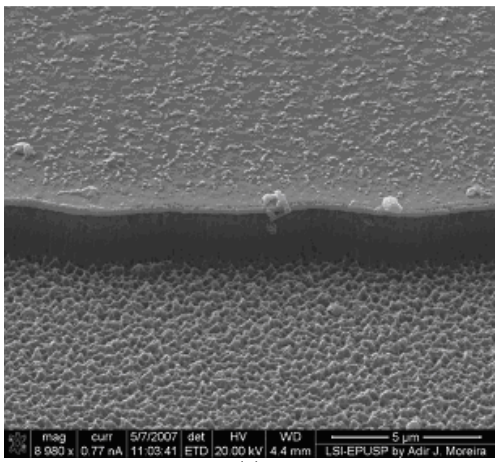

(c)

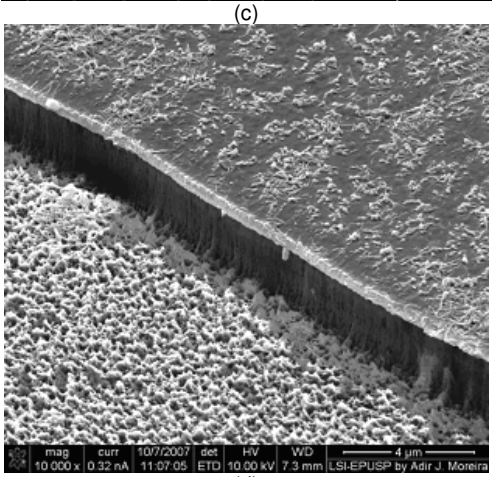

(d)

Figure 11. SEM micrographs of etched films that have gone through different chemical treatments: trichloroethylene, acetone and isopropyl alcohol (a); standard RCA process (b); 30 minutes in a potassium hydroxide solution (KOH) (c); and 10 seconds in a Buffered Oxide Etching (BOE) solution (HF + NH_4F (1:6)) (d).

Though the chemical treatments presented here did not result in any sidewall roughness improvement, it is important to point out the importance of the partial removal of the grass structure, which can compromise the fabrication of devices where metal films must be deposited over the structures. Other tests are being carried to improve sidewall roughness where the chromium mask is replaced by 5 µm SU8 photoresist in the etching process. These tests are not conclusive yet since the resist/film selectivity does not seem to be very high with the gases used in our RIE system. Also, polymer formation during the process seems to be slowing the etching process down. To overcome these difficulties we intend to use other gases (such as CF_4 and H_2) in the etching process in order to try to improve the selectivity.

Conclusions

Results of the fabrication and characterization of ARROW waveguides using sputtered TiO_x and a-SiC:H films as anti-resonant layer, have been presented in this work. Propagation losses as low as 0.87 dB/cm (TiO_2 waveguides) for multi-mode and 2.24 dB/cm for single-mode waveguides, were obtained.

Comparison between measured propagation losses with calculated ones and literature results indicate that the propagation losses in these waveguides are mostly due to scattering and can be further improved with changes in the fabrication process.

This problem was addressed with two different approaches: the use of different chemical treatments, which did not result in significant improvements and also by testing another masking material (SU8 photoresist) for the definition of the sidewalls. Though the latter approach is still not conclusive, we believe that it could lead to smaller losses.

Acknowledgements

This work was financially supported by FAPESP, CNPq and CAPES.

References

[1] R. Bernini, et al., Anal. Bioanal. Chem., Vol. 86, pp. 1267-1272, 2006.
[2] J. A. Plaza et al., Journal of microelectromechanical systems, Vol. 13, pp. 355-364, 2004.
[3] M. W. Ian et al., Applied Physics Letters, Vol. 89, pp. 191106, 2006.
[4] M.A. Duguay, Y. Kokubun, T.L. Koch and L. Pfeiffer, Appl. Phys. Lett , Vol. 49, pp. 13-15, 1986.
[5] Y. Kokubun and S. Asakawa, IEEE Photonics Technology Letters, Vol. 5, pp. 1418-1420, 1993.
[6] T. Lee, S.C. Hagness, D. Zhou, L.J. Mawst, IEEE Photonics Technology Letters, Vol. 13, pp. 770-772, 2001.
[7] H. Schmidt, D. Yin, J. P. Barber, and A. R. Hawkins, IEEE Journal of Selected Topics in Quantum Electronics , Vol. 11, pp. 519-527, 2005.
[8] D. O. Carvalho and M. I. Alayo, Journal of Optics A, Pure and Applied Optics, Vol. 10, pp. 104002, 2008.
[9] D. O. Carvalho and M. I. Alayo, 23rd Symposium on Microelectronics Technology and Devices (SBMicro 2008), The Electrochemica Society, Vol. 14, n. 1, pp. 511-520, Gramado, Brazil, 2008.
[10] P. K. Tien, Applied Optics , Vol. 10, pp. 2395-2413,1971.
[11] C. W. Tee, C. C. Tan and S. F. Yu, IEEE Photonics Technology Letters, Vol. 15, pp. 1231-1233, 2003.
[12] C.M.Kim and R.V.Ramaswamy, Journal of Lightwave Technology, Vol. 7, pp. 1581, 1989.
[13] H.A.Jamid, IEEE Microwave Guided Wave Lett. , Vol. 10, pp. 356, 2000.
[14] P.K. Tien, Applied Optics , Vol. 10, pp. 2395, 1971.
[15] D.Criado, I.Pereyra and M.I.Alayo, Materials Characterization, Vol. 50, pp. 167, 2003.
[16] I.Pereyra and M.I.Alayo,, Journal of Non-Crystalline Solids, Vol. 212, pp. 225-31, 1997.
[17] Y.T.Kim, et al., Surface and Coatings Technology, Vol. 171, pp. 34-38, 2003.
[18] P.Temple-Boyer, B.Hajji, J.L.Alay, J.R.Morante and A.Martinez, Sensors and Actuators A-Physical, Vol. 74, pp. 9, 1999.

[19] M.N.P.Carreño, J.P.Bottechia and I.Pereyra, Thin Solid Films , Vol. 308, pp. 219, 1997.
[20] M.I.Alayo, D.Criado, M.N.P.Carreño and I.Pereyra, Materials Science and Engineering B, Vol. 112, pp. 154–159, 2004.
[21] M.I.Alayo, D.Criado, L.C.D.Gonçalves and I.Pereyra, Journal of Non Crystalline Solids, Vol. 76, pp. 76, 2004.
[22] H.P.Uranus, H.J.W. M.Hoekstra and E.van Groesen, Optics Communications, Vol. 260, pp. 577, 2006.
[23] N.Daldosso, et al., Journal of Lightwave Technology, Vol. 22, pp. 1734, 2004.
[24] L. Zhou, F. Luo, M. Cao, Thin Solid Films, Vol. 489, pp. 229 – 234, 2005.